Supporting Information

An organic-inorganic hybrid photoluminescent ferroelastic with high phase transition temperature

Wen-Li Yang, Xin Yan, Miao Wang, Hao Yuan, Yuan-Yuan Tang, Yan Qin* and Xian-Jiang Song*

Ordered Matter Science Research Center, Nanchang University, Nanchang 330031, People's Republic of China.
Email: songxj@ncu.edu.cn

Measurement methods

Powder X-ray Diffraction. PXRD data were obtained through a Rigaku D/MAX 2000 PC X-ray diffraction system with Cu Kα radiation in the 2θ range of 10°-45° with a step size of 0.02° and a scan rate of 10°/min. Simulated powder patterns of samples were calculated by Mercury software package using the crystallographic data obtained from Single-crystal X-ray diffraction.

Single-Crystal X-ray Diffraction. Single-crystal X-ray diffraction data were collected using a Rigaku Saturn 924 diffractometer with Mo-Kα radiation (λ = 0.71073 Å). Rigaku CrystalClear 1.3.5 was used to perform the process of data collection, cell refinement and data reduction. Besides, the crystal structures were solved by direct methods and refined by the full matrix method based on F^2 using the SHELXLTL software package. The crystallographic data and structure refinement are summarized in Table S1-S3. The X-ray crystallographic structures have been deposited at the Cambridge Crystallographic Data Centre (deposition numbers CCDC: 2370180 and 2370182) and can be obtained free of charge from the CCDC via www.ccdc.cam.ac.uk/getstructures.

Thermogravimetric analyses (TGA). TGA were carried out on a PerkinElmer TGA 8000 instrument by heating crystalline samples from 300 K to 900 K with a rate of 30 K min^{-1} under a nitrogen atmosphere.

Differential scanning calorimetry (DSC) measurements. DSC measurements were performed with a NETZSCH DSC 200F3 instrument by heating and cooling the crystalline samples. The

measurements were carried out under nitrogen at atmospheric pressure in aluminium crucibles with heating and cooling rates of 20 K min^{-1}.

Dielectric measurements. Complex dielectric permittivities were measured with a TH2828A impedance analyzer. Silver conductive paste deposited on the plate surfaces of samples were used as top and bottom electrodes.

Ferroelastic measurements. The precursor solution of [TMIm][$MnCl_4$] was prepared by dissolving 10 mg of the crystals in 500 μL methanol. Then, a 20 μL precursor solution was spread on a clean indium doped tin oxide (ITO) glass substrate. The thin films were prepared by heat treatment at 313 K for 60 min and then annealed at 463 K for 5 min. Surface morphology and ferroelastic domain observations of thin films were performed on an Olympus BX53-P polarized light microscope.

Photoluminescence spectroscopy. The emission and excitation spectra of powder samples were measured using a Fluorolog-QM spectrophotometer (Horiba) equipped with a Xenon lamp as the excitation source. The time-resolved spectra were recorded through the same system equipped with a flash Xenon lamp as the excitation. The photoluminescence quantum yield was measured using an integrating sphere accessory. The variable temperature photoluminescence spectra were collected in the spectrofluorometer equipped with liquid nitrogen cryostat (V-100, Physike).

Table S1. Crystallographic data and refinement for [TMIm][$MnCl_4$].

Formula	$C_7H_{18}N_2Cl_4Mn$	
Temperature	293 K	453 K
Formula weight	326.97	326.97
Crystal system	Monoclinic	Orthorhombic
Space group	$P2_1/c$	*Pmmn*
a / Å	11.1678(6)	9.4512(9)
b / Å	9.3158(5)	11.3124(12)
c / Å	13.5838(6)	6.8298(7)
α (deg)	90	90
β (deg)	91.710(4)	90
γ (deg)	90	90
V / Å ^{3}	1412.59(12)	730.21(13)
Z, ρ_{calcd}/ g cm^{-3}	4, 1.537	2, 1.487
F (000)	668.0	334.0
Goodness-of-fit on F^2	1.044	1.075
R_1[a] (> 2σ)	0.0580	0.0713
wR_2[b] (> 2σ)	0.1364	0.2128

[a] $R_1 = \mathbf{\Sigma}||F_o| - |F_c||/\mathbf{\Sigma}|F_o|$, [b] $wR^2 = [\mathbf{\Sigma}(|F_o|^2 - |F_c|^2) / \mathbf{\Sigma}|F_o|^2]^{1/2}$

Table S2. Bond length (Å) and bond angle (°) of [TMIm][$MnCl_4$] at 293 K.

Bond Length (Å)		Bond Angle (°)	
Mn1-Cl1	2.3642(10)	Cl1-Mn1-Cl4	109.60(4)
Mn1-Cl2	2.3578(10)	Cl2-Mn1-Cl1	108.91(4)
Mn1-Cl3	2.3632(9)	Cl2-Mn1-Cl4	110.18(4)
Mn1-Cl4	2.3604(9)	Cl3-Mn1-Cl1	111.07(4)
N2-C1	1.497(5)	Cl3-Mn1-Cl2	105.61(4)
N1-C2	1.492(4)	Cl3-Mn1-Cl4	111.38(4)
N2-C4	1.495(4)	C1-N2-C5	108.8(3)
N1-C3	1.505(4)	C1-N2-C7	111.1(3)
N1-C4	1.508(4)	C4-N2-C1	110.2(3)
N2-C5	1.503(4)	C4-N2-C5	112.2(3)
C6-C7	1.500(5)	C4-N2-C7	103.0(2)
N1-C6	1.519(4)	C5-N2-C7	111.5(3)
N2-C7	1.511(4)	C2-N1-C3	109.6(3)
		C2-N1-C4	111.8(3)
		C2-N1-C6	110.6(3)
		C3-N1-C4	108.9(2)
		C3-N1-C6	109.8(3)
		C4-N1-C6	106.1(2)
		N2-C7-C6	103.2(2)
		N2-C4-N1	106.6(2)
		N1-C6-C7	103.6(2)

Table S3. Bond length (Å) and bond angle (°) of [TMIm][$MnCl_4$] at 453 K.

Bond Length (Å)		Bond Angle (°)	
Mn1-Cl2[1]	2.329(15)	Cl2[1]-Mn1-Cl2	116.6(9)
Mn1-Cl2	2.329(15)	Cl2[1]-Mn1-Cl1[1]	105.3(4)
Mn1-Cl1[1]	2.405(8)	Cl2-Mn1-Cl1[1]	105.3(4)
Mn1-Cl1	2.405(8)	Cl2[1]-Mn1-Cl2A[1]	5.8(11)
Mn1-Cl2A	2.39(2)	Cl2-Mn1- Cl2A[1]	110.8(7)
Mn1-Cl2A[1]	2.39(2)	Cl2A-Mn1-Cl1	107.8(6)
Mn1-Cl1A[2]	2.271(18)	Cl2A[1]-Mn1-Cl1	107.8(6)
Mn1-Cl1A	2.271(18)	Cl1A[2]-Mn1-Cl1A	8(2)
Mn1-Cl1A[3]	2.271(18)	Cl1A[1]-Mn1-Cl1A	91.2(15)
Mn1-Cl1A[1]	2.271(18)	Cl1A[3]-Mn1-Cl1A	90.7(16)
N1-C2	1.491(5)	C2-N1-C4	113.4(5)
N1-C3	1.480(13)	C2-N1-C4[4]	113.4(5)
N1-C4	1.500(7)	C2-N1-C3A[4]	103.7(4)
N1-C4[4]	1.500(7)	C2-N1-C3A	103.7(4)
N1-C3A[4]	1.513(12)	C2-N1- C4A	107.3(8)
N1-C3A	1.513(12)	C2-N1-C4A[4]	107.3(8)
N1-C4A	1.511(14)	C3-N1-C2	109.1(4)
N1-C4A[4]	1.511(14)	C3-N1-C4[4]	95.6(8)
C3-C3[3]	1.503(10)	C3-N1-C4	95.6(8)
C3A-C3A[3]	1.533(7)	C3-N1-C3A[4]	34.0(3)
Cl1A-Cl1A[2]	0.31(8)	C3-N1-C4A[4]	127.0(11)
		C4-N1-C4[4]	124.6(13)
		C4-N1-C3A[4]	66.6(9)
		C4[4]-N1-C3A[4]	126.3(8)
		C4-N1-C4A[4]	103.8(15)
		C4[4]-N1-C4A[4]	33.8(6)
		C4A[4]-N1-C3A	100.4(11)
		C4A-N1-C3A	148.8(9)
		N1[5]-C2-N1	106.7(5)
		N1-C3-C3[3]	107.5(3)
		N1-C3A-C3A[3]	106.5(2)
		Cl1A[2]-Cl1A-Mn1	86.1(10)

Figure S1. The experimental PXRD pattern of [TMIm][$MnCl_4$] at 298 K matches well with its simulated PXRD pattern.

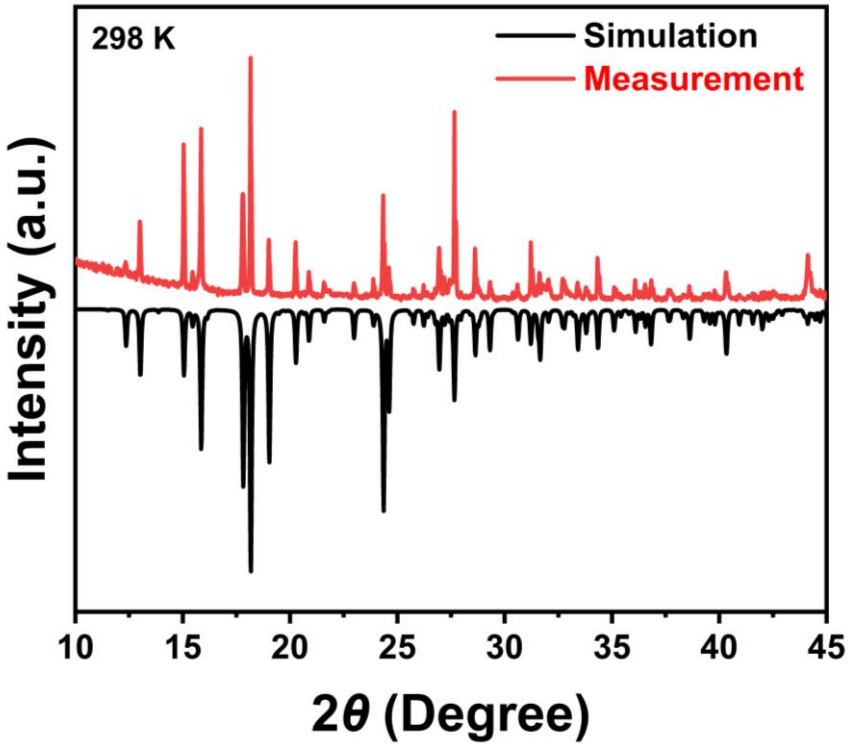

Figure S2. The PXRD pattern of [TMIm][$MnCl_4$] thin film at 298 K.

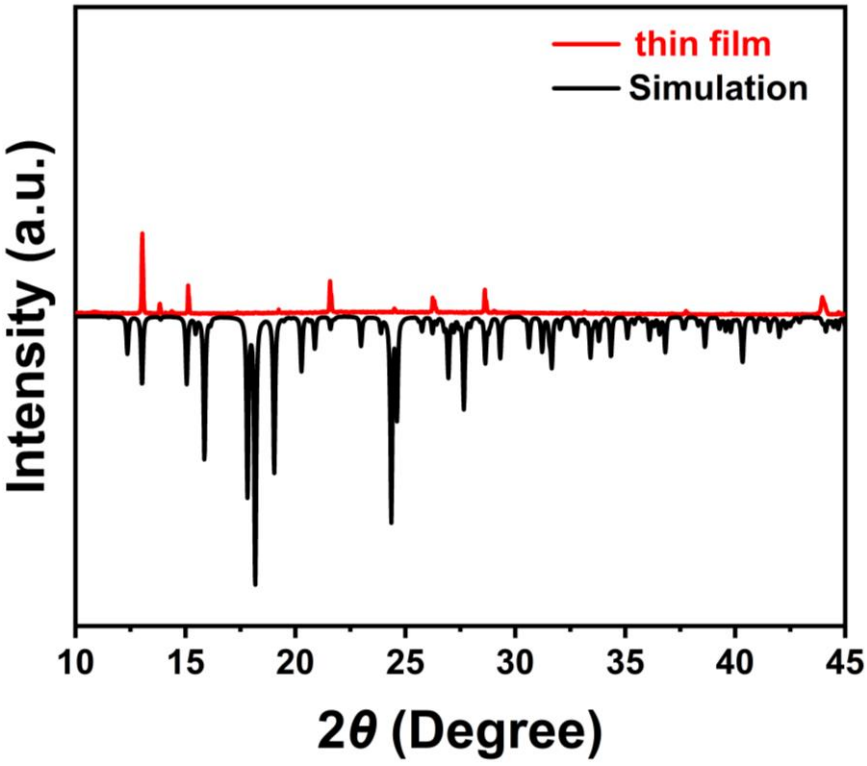

Figure S3. TGA curves of [TMIm][$MnCl_4$].

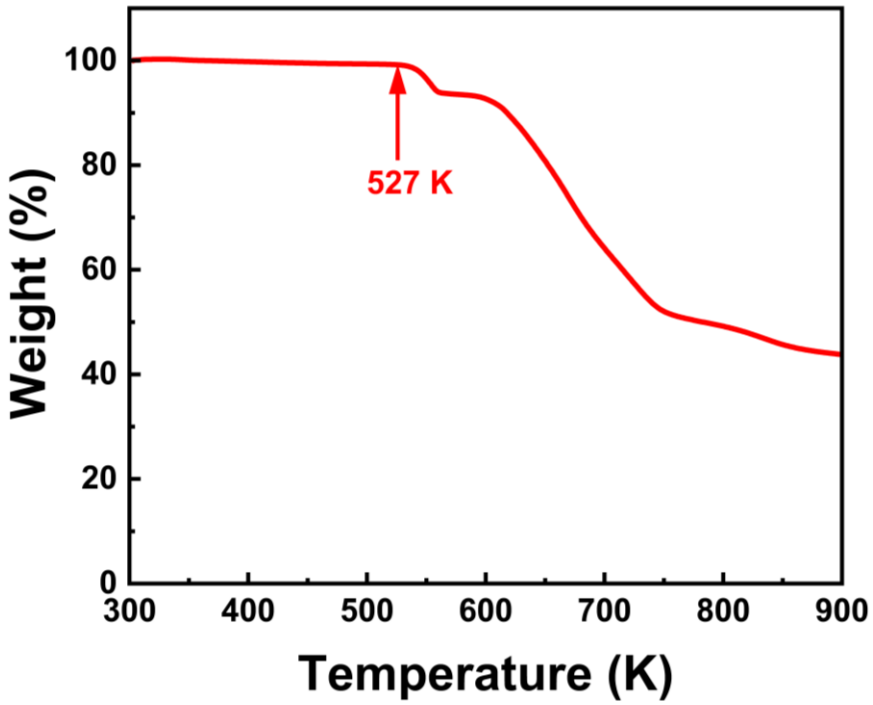

Figure S4. The variation of ε' at 100 kHz during the heating and cooling process.

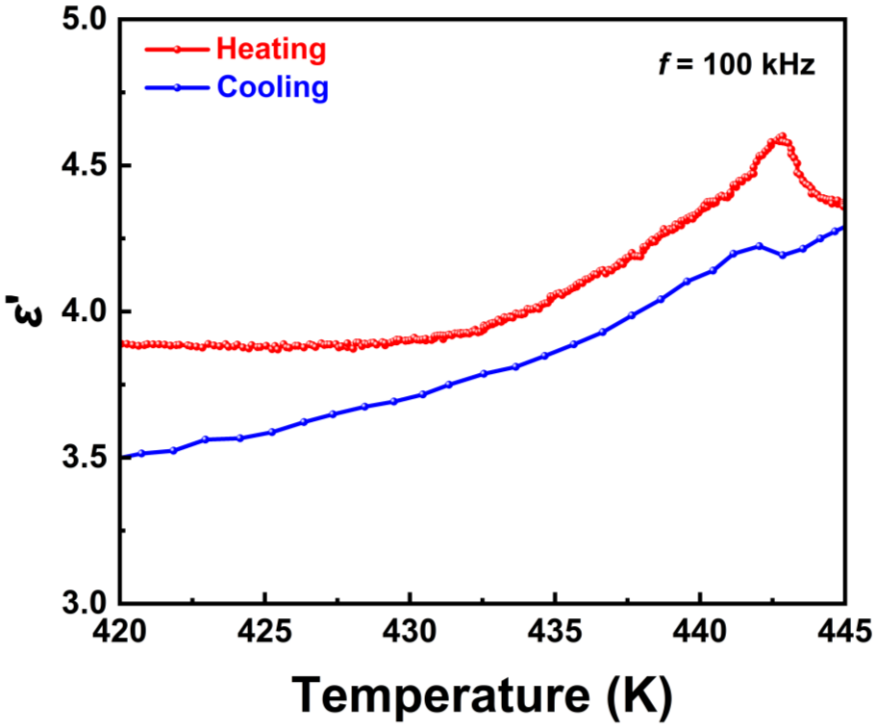

Figure S5. The PL quantum yield of [TMIm][$MnCl_4$] at room temperature.

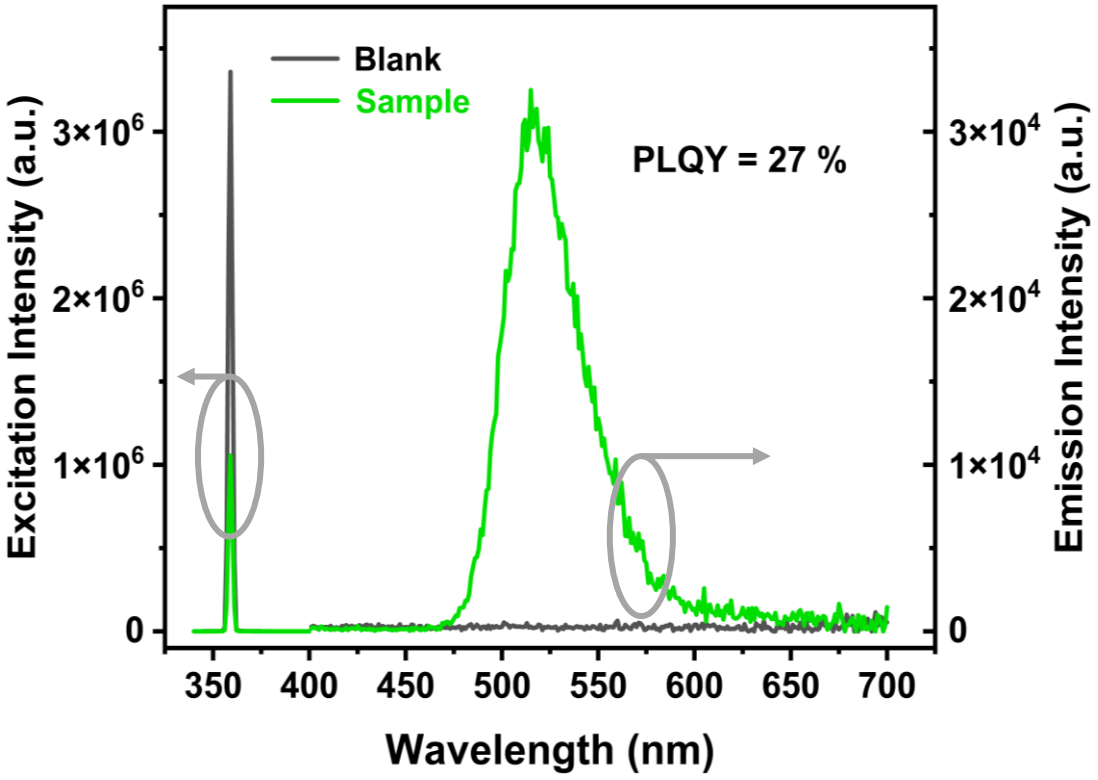

Figure S6. The variation of peak center with temperature in VT-PL spectra of [TMIm][$MnCl_4$].

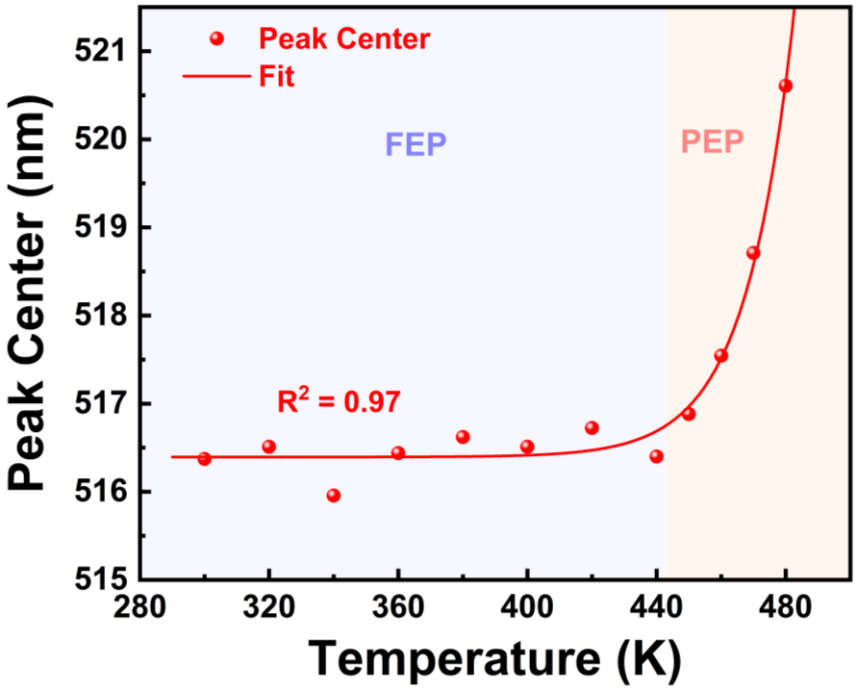

Figure S7. The variation of the full width at half maximum with temperature in VT-PL spectra of [TMIm][$MnCl_4$].